In-Core Neutron Detection System Using a Dual-Mode Self-Reset Preamplifier With the Micro-Pocket Fission Detector

Minuk Seung, Duckhyun Kim, Dongseong Shin, Troy C. Unruh, Kevin Tsai, Woo-Young Choi, *Member, IEEE*, and Inyong Kwon, *Member, IEEE*

***Abstract*— This article presents the development of an in-core neutron detector readout system utilizing a charge-sensitive amplifier (CSA) with a self-reset technique, alongside data loggers, to measure the output of the CSA. Micro-pocket fission detectors (MPFDs) were developed as in-vessel neutron detectors having many advantages in terms of portability size, reproducibility of charge deposition, usability in high neutron flux, and capability of gamma-ray discrimination. The proposed readout system for MPFDs can be operated in a dual mode which consists of integration and single event modes. The integration mode can count the number of saturated preamplifier outputs in a high-radiation environment. On the other hand, the single-event mode can directly measure the analog data induced by detectors. A novel approach to dead time compensation is also introduced using an active dead time control (ADTC) method. This article shows the reactor transient test results conducted at the transient reactor test (TREAT) reactor. The neutron flux of 7×10^{15} n/cm^2·s with the full-width half maximum (FWHM) of 126 ms at the reactor power of 2.1 GWth was measured. According to the reactor power of 5.1 GWth, the neutron flux and FWHM were obtained as 1.24×10^{16} n/cm^2 · s and 136 ms, respectively.**

***Index Terms*— Active dead time control (ADTC), charge-sensitive amplifier (CSA), integrated circuit (IC), micro-pocket fission detectors (MPFDs), MPFDs readout system, neutron fission detector, reactor instrumentation, self-reset preamplifier.**

I. Introduction

MODERN commercial nuclear power plants (NPPs) have various instruments to enhance the reliability and safety of their operations. These instruments include radiation detectors, thermometers, and pressure gauges [1], [2]. Most of all, understanding the power profile of NPPs is essential for their economical and reliable operation. This profile is generally assessed using neutron detectors, such as ion chambers located outside the reactor. The neutron detector response is usually supposed to be proportional to the neutron flux. However, ex-vessel detectors could be inefficient as they can measure only leakage neutrons from the vessel [3]. Previous studies have shown an error of 15% when using the ex-core ion chamber to measure the reactor power distribution [4]. Therefore, the use of in-core detectors is required for accurately monitoring the reactor flux profile.

In addition to detectors located in a reactor, the size of detectors should be significantly minimized for small modular reactors (SMRs) that have recently been developed for producing electricity less than 300 MWe [5]. SMRs offer many advantages in terms of cost, flexibility, reliability, and reduced risk of sabotage [6]. However, monitoring the flux profile of SMRs using ex-core detectors is challenging due to the limited number of neutrons leaking from the vessel, a characteristic resulting from enhanced propagation resistance which is one of the advantages of the SMR [7]. Traditional in-core fission chambers might not be suitable for SMR applications because of their limited device lifetime and susceptibility to large flux perturbations [8].

Micro-pocket fission detectors (MPFDs) were developed and verified by Kansas State University and Idaho National Laboratory (INL) for several years [9], which were designed to measure the neutron flux inside of the reactor in real-time. As reported in previous studies, small-size detectors have many advantages as in-core detectors in terms of small size, usability in high neutron flux, uniform charge deposition, and gamma-ray discrimination capability [10], [11], [12], [13]. To realize the in-core neutron detector for monitoring power distribution, a readout system should be designed to be fit for the MPFDs. Previous research had focused on using discrete components for readout system [14]. However, the commercial components have drawbacks including large area, high power dissipation, and complex design for miniaturized applications. Consequently, the MPFDs readout system needs to be redesigned by using application-specific integrated circuits (ASICs) to overcome these limitations.

A charge-sensitive amplifier (CSA) is widely used as a preamplifier for various radiation detector systems, such as ion chambers, scintillator detectors, and fission chambers [15], [16]. The output of the MPFDs is generated as the charge form, the CSA can be used for converting current to voltage

Manuscript received 29 May 2023; revised 1 September 2023; accepted 9 September 2023. Date of publication 25 September 2023; date of current version 20 October 2023. This work was supported in part by the Basic Science Research Program through the National Research Foundation of Korea (NRF) Funded by the Ministry of Science and Information and Communication Technology (MSIT) under Grant RS-2022-00144324, Grant 2022M3F3A2A01072855, and Grant 2020M2A8A1000830. The Associate Editor coordinating the review process was Dr. Carlos G. Juan. *(Corresponding author: Inyong Kwon.)*

Minuk Seung is with the Korea Atomic Energy Research Institute (KAERI), Daejeon 34057, South Korea, and also with the College of Electrical and Electronic Engineering, Yonsei University, Seoul 03722, South Korea (e-mail: mseung@yonsei.ac.kr).

Duckhyun Kim and Dongseong Shin are with the Korea Atomic Energy Research Institute (KAERI), Daejeon 34057, South Korea (e-mail: duck@kaeri.re.kr; sds@kaeri.re.kr).

Troy C. Unruh and Kevin Tsai are with the Idaho National Laboratory (INL), Idaho Falls, ID 83415 USA (e-mail: troy.unruh@inl.gov; kevin.tsai@inl.gov).

Woo-Young Choi is with the College of Electrical and Electronic Engineering, Yonsei University, Seoul 03722, South Korea (e-mail: wchoi@yonsei.ac.kr).

Inyong Kwon is with the Department of Radiological Science, Yonsei University, Wonju 26493, South Korea (e-mail: ikwon@yonsei.ac.kr).

Digital Object Identifier 10.1109/TIM.2023.3318685

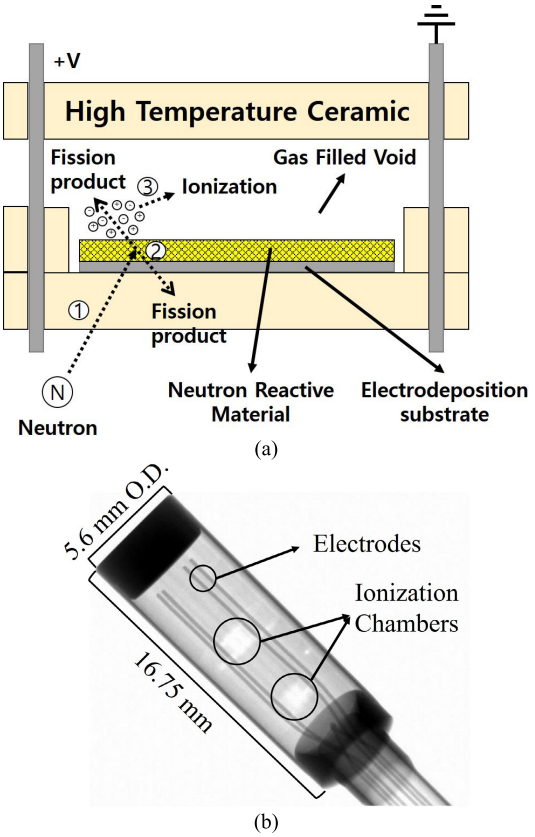

Fig. 1. Prototype MPFD structure is shown with active fission area. (a) Neutron reactive material as a fissile layer generates fission fragments of which energy is deposited by interacting with Argon gas [14], [19]. (b) X-ray image of the single MPFD [14].

as a preamplifier [17]. However, a pile-up phenomenon can be observed with the general-purpose CSA in a high-radiation environment [18]. Since the CSA output is proportional to the amount of input charges, if the response of the MPFDs is significantly faster than the discharge period of the CSA in the high-power nuclear reactor, charges can be consistently cumulated at the feedback capacitor of the CSA. Then, the preamplifier output can be saturated to the maximum value. Eventually, the sensor interface cannot read the accurate signal. Therefore, this work aims to design the first MPFDs readout system by using the ASIC to measure the high flux neutron distribution as an in-core detector. The sensor interface is designed, including the preamplifier with a self-reset technique, data loggers for processing data, and a remote monitoring algorithm for real-time measurement.

II. MDPFs Readout System Design

The prototype MPFDs are displayed in Fig. 1 [14], [19]. The detector design consists of multiple nodes coated by varying enrichments of uranium fissile materials, which have less than 1 μm thickness, to interact with fast neutrons and thermal neutrons in the reactor [9], [10]. When a neutron interacts with the neutron reactive material, fission can occur, resulting in the production of fission products. These fission products can cause ionization reactions within gas-filled void regions. The ions generated during this process then flow along the electrodes.

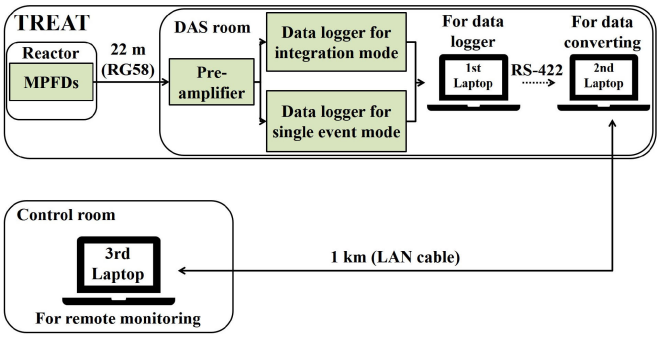

Fig. 2. Overall MPFD readout system block diagram. The system consists of the preamplifier, two data loggers for integration mode and single event mode operations, and the laptop for monitoring measured data in real time.

The overall MPFDs readout system is shown in Fig. 2. This system is located inside the reactor of the transient reactor test (TREAT) at INL. To minimize the effects of radiation, the readout system is installed in a separate data acquisition system (DAS) room, located away from the reactor. The MPFDs signal is transmitted along an RG58 cable to the preamplifier. Two laptops are located in the DAS room. One laptop is used for controlling the data loggers, while the other laptop is utilized to process the acquired data and present neutron flux on the user interface. These two laptops communicate with each other using the RS-422 wireless communication protocol at a consistent time interval of 10 ms. The second laptop is connected to the third laptop in the control room via the LAN cable, allowing for real-time monitoring of the reactor transient from a distance of 1 km.

A. Readout System Operation Principle

The readout system operates in two detection modes: single event and integration. The single event mode can measure the analog data at the output of the preamplifier. On the other hand, the integration mode is utilized in a high radiation environment, such as the inside of the reactor, and merged with the current mode and count mode detectors [20], [21]. The distinction between the current mode and the integration mode lies in their measurement approach. In the current mode, the average current is measured, whereas in the integration mode, this is not the case. Instead, the proposed readout system maintains a constant charge on the feedback capacitor of the preamplifier. Whenever the output of the preamplifier is saturated in the high radiation field, the data logger for the integration mode counts the number of saturations of the CSA as the count mode detector. The remote monitoring system displays the neutron count rate using the measured data.

B. Preamplifier Design With Self-Reset Technique

The operation principle of the CSA is that the input charges induced from radiation detectors are stored in the feedback capacitor (C_F) and converted into the output voltage as determined by the following equation [22]:

$$V_{\text{out}} = -A_V \frac{Q_{\text{in}}}{C_{\text{det}} + (A_V + 1)C_F} \tag{1}$$

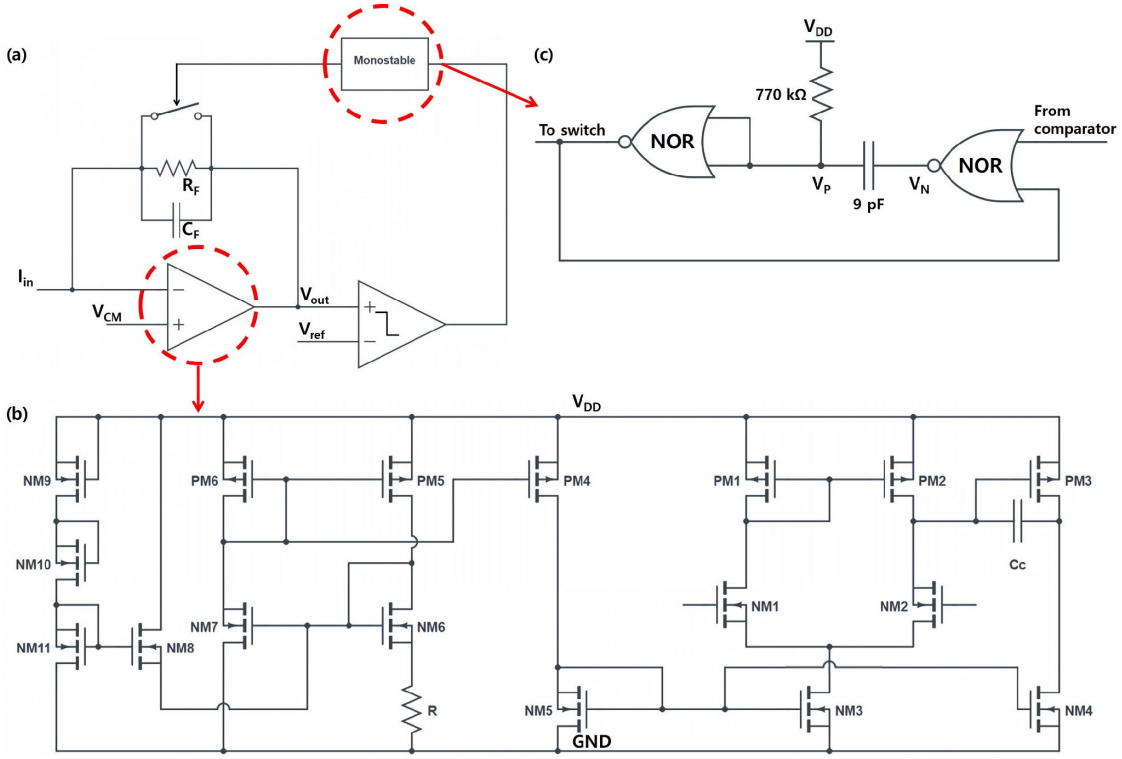

Fig. 3. (a) Proposed preamplifier diagram including OPAMP, feedback network, comparator, and monostable circuit. (b) Conventional two-stage OPAMP topology. (c) Monostable circuit diagram.

where A_V is the open loop gain of the OPAMP and C_{det} is the detector capacitance. When C_{det} is lower than $(A+1)C_F$, the equation can be simplified as written by the following equation [23]:

$$V_{\text{out}} = -\frac{Q_{\text{in}}}{C_F}. \tag{2}$$

As aforementioned, the self-reset technique is applied to compensate for the output saturation in the high radiation field. The proposed preamplifier consists of the following circuits: CSA, comparator, monostable circuit, and feedback network, including a switch to reset saturated signals, as shown in Fig. 3(a). The two-stage operational amplifier (OPAMP) with a self-bias circuit is used for the CSA. The two-stage OPAMP is well known for its high speed, low noise, low power, and proper gain. Fig. 3(b) displays the schematic of the two-stage OPAMP. The feedback components are a capacitor of 0.75 pF and a resistor of 2 MΩ. Thus, the time constant is calculated as 1.5 μs. The value of each component is set by using an electronic design automation (EDA) tool. The feedback gain of the CSA is defined as the inverse of the feedback capacitance. A low feedback capacitance can allow the CSA to achieve a high feedback gain. However, it can quickly saturate the output of the CSA in the high radiation field, leading to a degradation in count rate. In terms of resistor, the feedback resistor is for discharging the capacitor after completion of the input signal conversion. The value of this resistor should be sufficiently large to ensure that all the charges inputted are stored on the feedback capacitor. However, if the resistance is too large, it can increase the *RC* time constant, resulting in a longer discharge time. Moreover, passive components can undergo the process variation during the fabrication. Therefore, the feedback components are used at the printed circuit board (PCB) level after being validated through EDA simulation.

TABLE I
ELECTRICAL PARAMETERS OF THE OPAMP

Design Specifications	Value
Supply voltage	1.8 V
Miller capacitance (Cc)	1 pF
Gain (dB)	66
3dB BW (kHz)	112.5
GBWP (MHz)	217.15
PM (°)	55

Table I shows the specifications of the OPAMP for the CSA. The preamplifier could operate as a conventional CSA in a low-radiation environment. On the other hand, when the preamplifier is used during high radiation events, the output of the CSA becomes larger than the reference voltage of the comparator due to the pile-up phenomenon. Subsequently, the continuous comparator produces a reset signal employed by the monostable circuit to detect the input signal and trigger the feedback switch.

The monostable circuit comprises two NOR gates and an *RC* network, as depicted in Fig. 3(c). It operates under the law of conservation of charge. As shown in Fig. 4, when the HIGH signal of the comparator enters the monostable input, the output voltage V_N of the NOR gate goes LOW and V_P also goes to LOW due to the charge conservation.

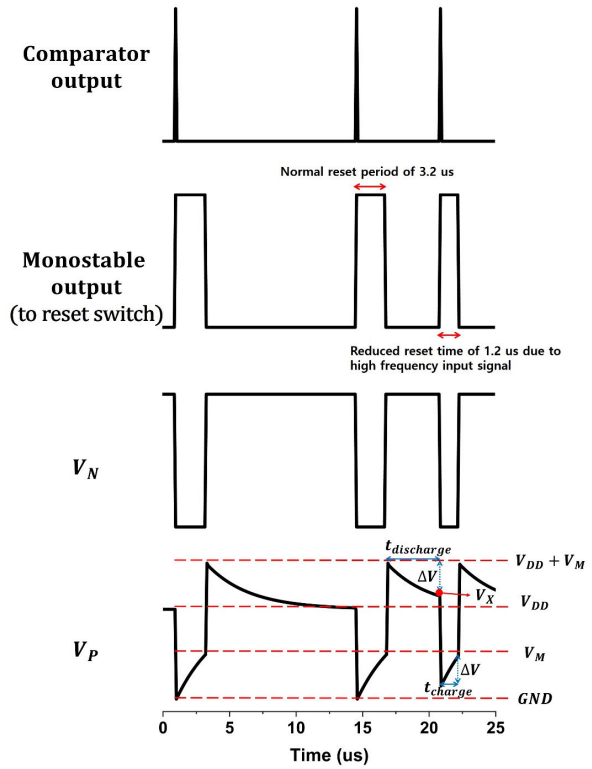

Fig. 4. Operation principle of monostable circuit. When comparator signal enters monostable, the monostable output is generated. If discharge time is not sufficient due to high frequency input signals, the reset time will decrease.

Even if the input returns to LOW, the capacitor charges slowly, allowing the monostable output to remain HIGH. V_P increases to V_M, which is the voltage where the second NOR gate transition occurs, upon charging. The monostable output becomes LOW, provided to the first NOR gate, and V_N goes to HIGH. Subsequently, the V_P also increases up to the voltage expressed in the following equation according to the charge conservation law:

$$V_P = V_M + V_{\mathrm{DD}}. \tag{3}$$

The capacitor is discharged slowly to V_{DD}, while the input of the NOR gate is zero.

The monostable circuit produces pulses with sufficient time to stabilize the system, even in process variations. During the reset phase, the charges stored in the feedback capacitor of the CSA may rapidly decrease, leading to instability caused by underdamping, occurring multiple up-and-down signals generated by the comparator that cause a malfunction of the self-reset technique. Thus, sufficient reset time can help minimize process variation and mismatch issues during the fabrication.

The reset time of the preamplifier is considered as a dead time of the system, causing the count rate degradation. However, the monostable circuit acts as an active dead time control (ADTC) circuit. For a complete reset, V_X should decrease to the V_{DD} in the discharge phase to maintain the constant pulsewidth. If the input signal speed is too high, V_X voltage may be higher than V_{DD}, namely insufficient discharge time, which reduces t_{charge} due to remaining charges. In other words, the dead time is actively controlled by the input period.

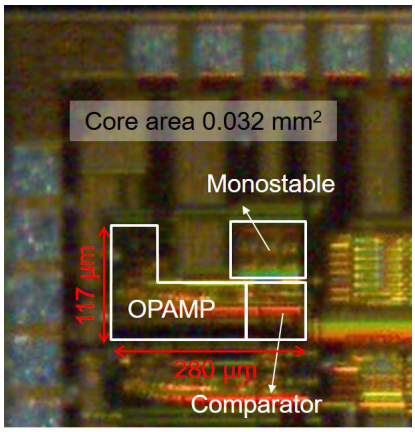

Fig. 5. Die photograph of the fabricated preamplifier.

TABLE II
PROPERTIES OF THE DATA LOGGER UNITS

Type	Digital	Analog
Channels	24	2
Sample rate	800 MS/s	100 MS/s
Bandwidth	100 MHz	10 MHz
Voltage range	1.2 V to 3.3 V	±25 V
Manufacturer	Digilent	

Consequently, the degradation of the count rate can be reduced by using the monostable circuit.

The proposed preamplifier was realized in a complementary 0.18 μm CMOS technology process. A die photograph of the fabricated chip is shown in Fig. 5. The active area of the proposed circuit occupies 0.032 mm^2. The power is consumed about 63 mW at the steady state.

C. Data Logger and Remote Monitoring System

The signal processing unit and remote monitoring system have been developed to monitor measured data in the TREAT facility's control room in real-time. Analog and digital data loggers are used to collect and process the preamplifier data in integration and single-event modes, respectively. Table II shows the properties of the data loggers, respectively.

Whenever the CSA is saturated, the comparator generates the pulse. The analog data logger can function as an oscilloscope, allowing for monitoring of the preamplifier output state and logging of analog data within a 1 ms time window. On the other hand, the digital data logger counts the number of pulses generated by the comparator every 10 ms for integration mode detection, and then transfers the data to the monitoring system for post processing from the count data to neutron flux. The software for the data loggers was provided by the manufacturer.

The remote monitoring system displays transient data acquired through the MPFDs readout system and reactor trigger signal on a PC in the control room. The user interface for remote monitoring utilized self-developed software. The monitoring system interface is shown in Fig. 6. The remote monitoring system receives cumulated data from the software for the data loggers over a duration of 10 ms. Users can set

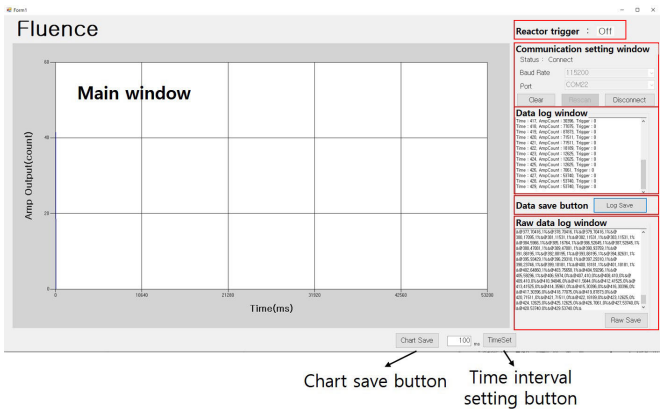

Fig. 6. Software interface of the MPFD readout system.

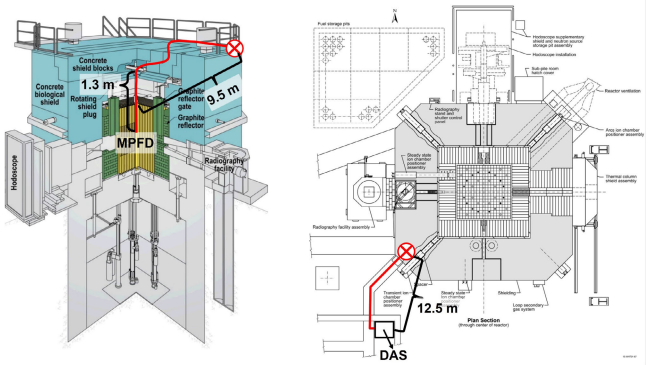

(a) (b)

Fig. 7. Overview of the TREAT facility. Reactor cross-sectional view. (a) Reactor bird-eye view. (b) Total distance from MPFDs to DAS is approximately 22 m.

the baud rate to the desired speed. The baud rate was set to 115 200 to obtain as much data as possible in this work. This program automatically detects and sets the USB port connecting the data logger. The data log window displays the parsed time and transferred data from the data logger. The main screen draws the count rate over time as a graph. All data, including the graph, can be stored on the laptop.

III. Verification Test for MPFDs Readout System

A. Test Environment

The MPFDs readout system verification test was conducted at the TREAT reactor at INL, an air-cooled research reactor capable of generating up to 20 GWth of thermal reactor power within approximately 300 ms [9]. The tests were conducted twice under conditions of 2.1 and 5.3 GWth, respectively. Fig. 7 provides an overview of the TREAT facility where the MPFDs are positioned in the reactor core. Signals of the MPFDs are transferred via a long cable of 22 m to the preamplifier in a DAS room inside TREAT to minimize the radiation effect on the system, as depicted in Fig. 8. The first laptop placed in the DAS room is connected to the second PC through the RS-422 communication protocol. For real-time monitoring, the second PC is controlled by the third PC located in the control room, which is approximately 1 km from the TREAT reactor, using the LAN cable. The DUT board has one preamplifier and a large coupling capacitor having a rated

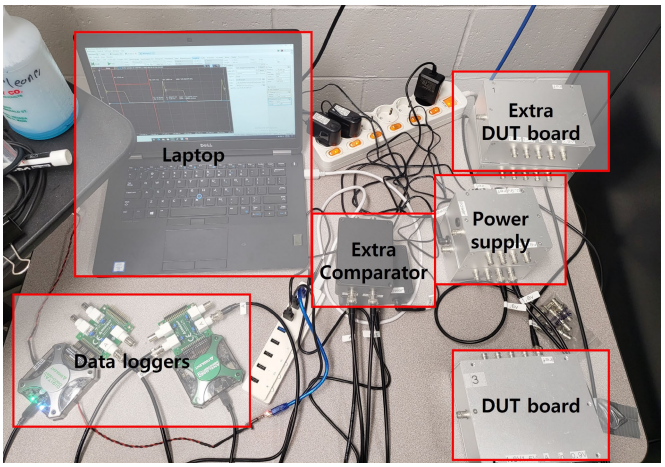

Fig. 8. Developed MPFD readout system was installed at DAS. The overall system consists of the following blocks: DUT board, extra comparator, power supply, data loggers, and laptop.

voltage of 1100 V to block the high supply voltage of 100 V at the input port. The additional comparator is installed to trigger the integration mode data logger, and the power supply box is used to minimize the overall system area.

B. Measured Pulses From a Reactor Transient Test

Fig. 9 illustrates the preamplifier output recorded during the reactor transient, revealing that the preamplifier becomes saturated due to the high neutron flux. Furthermore, the CSA undergoes an automatic reset whenever its output approaches 1.6 V, a reference voltage for the comparator that generates a reset signal. The saturation time and dead time are both dependent on the neutron flux. Specifically, in high neutron environments, the saturation period is relatively shorter, as illustrated in Fig. 9(a), 3.72 and 2.76 μs, respectively. On the other hand, as shown in Fig. 9(b), the rising time takes longer to saturate the CSA when the neutron flux is relatively low, 7.44 μs. Moreover, as mentioned before, the dead time is proportional to the input rising time due to the ADTC. Therefore, the dead time was measured as 2.04, 1.8, and 3 μs, respectively. As the test result, the range of the dead time is from 0.84 to 3.36 μs during the transient test according to the input frequency.

C. Transient Data Conversion Method

The obtained data need to be converted from the count rate to the neutron flux. The conversion of the MPFDs readout system was conducted using the following equation:

$$\varphi(\mathrm{n/cm^2 \cdot s}) = \frac{\alpha n}{S} \tag{4}$$

where α is the minimum number of neutrons required to saturate the CSA, n is the ideal count rate, and S is the sensitivity of MPFDs.

The sensitivity S of the MPFDs was investigated using the MCNP6 in a full energy range of the neutron for the natural uranium having 300 Å thickness as expressed in the following equation [9]:

$$S = 2.85 \times 10^{-9}\ \mathrm{cm^2}. \tag{5}$$

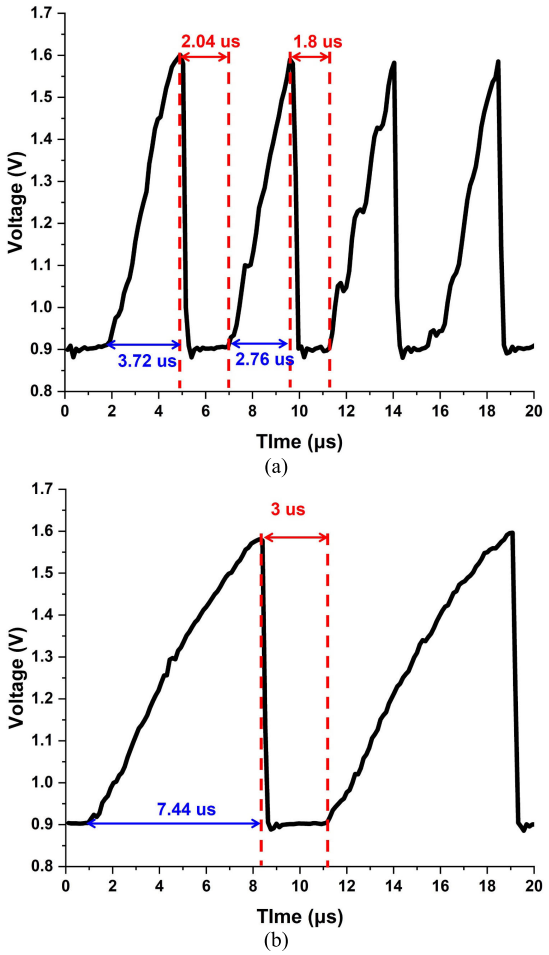

Fig. 9. Analog result of transient tests. The preamplifier is automatically reset whenever output is saturated. The input rising time is determined by neutron flux and dead time. (a) Since the neutron flux is relatively high, the input rising time is also fast and dead time is short. (b) Since the neutron flux is relatively low, input rising time is slow and dead time is long.

The α can be calculated as a ratio between the charge generated per reaction and the charge that can be stored in the circuit. The MPFDs are characterized by high repeatability in terms of charge generation, with approximately 20 fC charges generated per neutron interaction [14]. Since the input charges are deposited at the preamplifier up to 525 fC, which is calculated using (2), the minimum number of the pulse can be calculated as 27/saturation. Namely, α is 27. Moreover, the proposed system can reduce the deposited charge variation due to the advantages of the current mode of operation of the system [24].

The ideal count rate, n, is related to the dead time generated by electric circuits instead of the sensor in modern radiation detectors, including the MPFDs readout system [25]. Since the MPFDs readout system is considered the nonparalyzable model, following equation might be used for compensating the dead time in this work [18]:

$$n = \frac{m}{1 - m\tau_{\text{deadtime}}} \tag{6}$$

where m is the measured count rate. To obtain the actual count rate, it is essential to study the dead time. As previously mentioned, the ADTC circuit can generate pulses of varying widths depending on the input rising time. Therefore, the following steps outline the calculation method for determining the dead time. The discharge phase of the monostable is defined as (7). On the other hand, the charge phase is expressed as (8). The maximum charge time, denoted as $t_{\text{charge,max}}$, was determined to be 3.36 μs through experimental results

$$V_X = ((V_M + V_{\text{DD}}) - V_{\text{DD}})e^{-\frac{t_{\text{discharge}}}{\tau}} + V_{\text{DD}} \tag{7}$$

$$V_M = -V_{\text{DD}}e^{-\frac{t_{\text{charge,max}}}{\tau}} + V_{\text{DD}} = (V_X - 2V_{\text{DD}})e^{-\frac{t_{\text{charge}}}{\tau}} + V_{\text{DD}}. \tag{8}$$

Following equation is obtained by substituting (7) for (8) and rearranging the equation:

$$\frac{V_M}{V_{\text{DD}}}e^{\frac{-(t_{\text{discharge}}+t_{\text{charge}})}{\tau}} - e^{-\frac{t_{\text{charge}}}{\tau}} = \frac{V_M}{V_{\text{DD}}} - 1 \tag{9}$$

where τ is the RC constant of the monostable circuit. V_M and τ might be variated during the fabrication at a maximum rate of 30%. Thus, V_M and τ values should be investigated before $t_{\text{discharge}}$ and t_{charge} are calculated. V_M term can be eliminated by replacing (8) with (9), and then the τ is the only variable

$$e^{\frac{-(t_{\text{discharge}}+t_{\text{charge}})}{\tau}} - e^{\frac{-(t_{\text{discharge}}+t_{\text{charge}}+t_{\text{charge},max})}{\tau}} - e^{-\frac{t_{\text{charge}}}{\tau}} + e^{-\frac{t_{\text{charge,max}}}{\tau}} = 0 \tag{10}$$

$t_{\text{discharge}}$ can be expressed as the rising time of the input, and t_{charge} is identical to the dead time of the preamplifier. Equation (10) is solved using the data shown in Fig. 9(a). As the result, the RC-constant was calculated as 4.9883 μs, and V_M is 0.9178 V. The average period of a single saturated pulse could be obtained by dividing the analog data acquisition time into the count rate during the acquisition. Herein, it is necessary to establish the correlation between the pulse period and the dead time to compensate for the dead time degradation into total counts. The correlation is calculated by evaluating (10). The period is defined as the summation of the discharge and charge time. As mentioned above, the charge time of the monostable is replaced with the dead time. The exponential terms in (10) are replaced as shown in the following equation in order to simplify the calculation:

$$X = e^{-\frac{t_{\text{charge}}+t_{\text{discharge}}}{\tau}}, \quad Y = e^{-\frac{t_{\text{charge}}}{\tau}}. \tag{11}$$

Therefore, the correlation equation is obtained

$$Y = 0.49X + 0.51, \quad (0 < X, Y < 1). \tag{12}$$

The correlation graph between period and dead time is plotted as shown in Fig. 10, where the abscissa is the rising time of the average period, and the vertical axis is the dead time of the system. As the analysis result, the asymptotic line is drawn near 3.35 μs, similar to the maximum dead time of measured data during the transient test, as mentioned before. The exponential trend curve is drawn to derive the period in which the asymptotic line is 3.47 μs as expressed in the following equation:

$$\tau_{\text{dead time}}(\mu\text{s}) = -3.51e^{\left(-\frac{\text{avg. period}}{6.47\ \mu\text{s}}\right)} + 3.47. \tag{13}$$

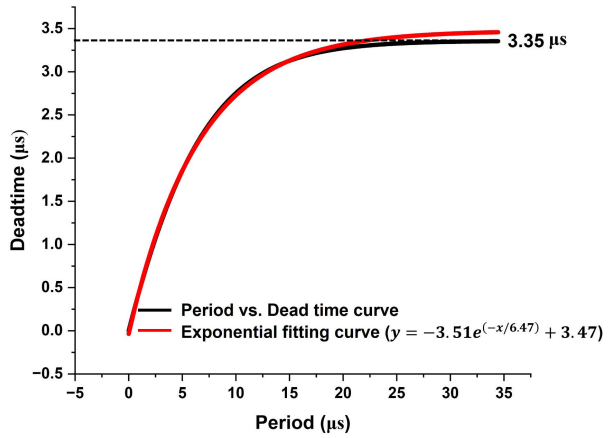

Fig. 10. Correlation curve between input period and dead time. Since the correlation curve follows exponential function, the curve approaches to asymptotic line of 3.35 μs. The exponential trend curve is used for obtaining dead time by using the count rate.

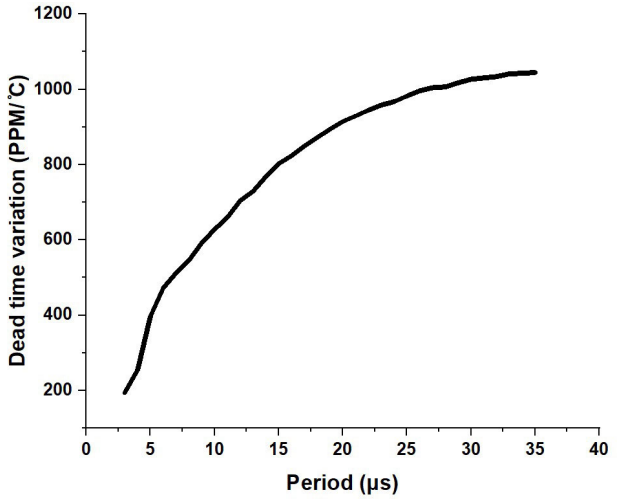

Fig. 11. Simulation result of temperature variation from −20 °C to 80 °C. The result shows how the dead time varies for each input period as the temperature changes. The investigation revealed that as the input period increases, the variation in dead time also increases.

Therefore, the dead time compensation is achieved by substituting (6) with (13), as shown in the following equation:

$$n = \frac{m}{1 + m(3.51e^{\left(-\frac{1\ \mu s}{m \times 6.47\ \mu s}\right)} - 3.47)}. \tag{14}$$

Fig. 11 shows the simulation results of dead time variations under temperature variations from −20 °C to 80 °C. The *x-axis* represents the input time period, while the *y*-axis displays the variation in dead time. The degree of dead time variation is directly proportional to the period, with a maximum rate of 1045 ppm/°C.

D. Neutron Flux Data Conversion

The neutron flux data underwent cubic interpolation to increase the data points for accuracy analysis. The data was then processed using the conversion method from count rate to neutron flux. Fig. 12 illustrates the results of the TREAT transient test, including measuring reactor power through existing

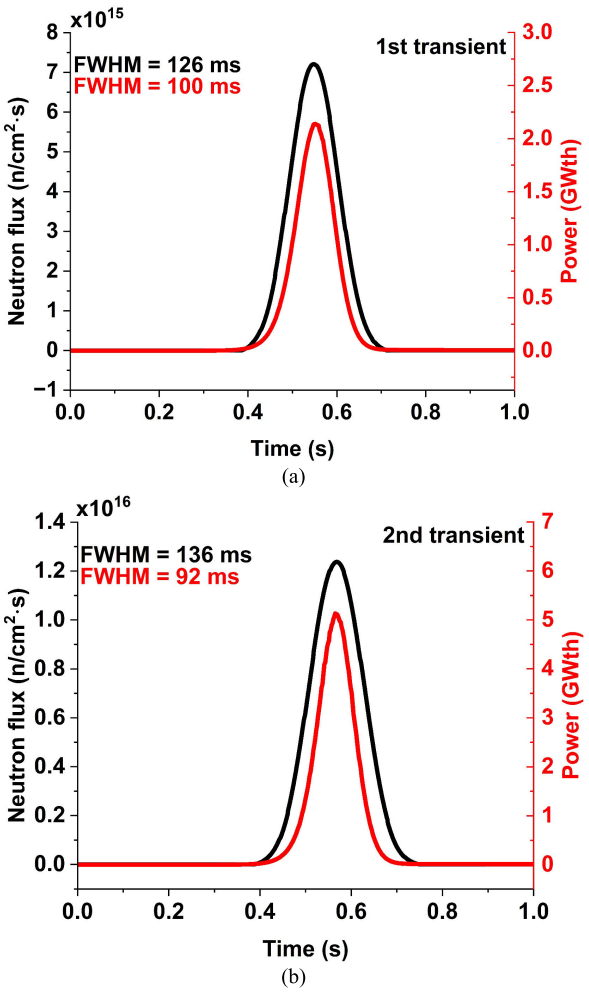

Fig. 12. Reactor transient test results of neutron flux and reactor power. (a) When reactor power is 2.1 GWth, measured neutron flux is 7.2×10^{15} n/cm$^2 \cdot$ s having FWHM of 126 ms. (b) When reactor power is 5.1 GWth, measured neutron flux is 1.24×10^{16} n/cm$^2 \cdot$ s having FWHM of 136 ms.

ex-core ion chambers positioned in the northwest, southwest, and southeast corners, as well as the neutron flux converted using the proposed method. The neutron flux was measured up to 7.2×10^{15} n/cm$^2 \cdot$s with full-width half maximum (FWHM) of 126 ms at the thermal power of 2.1 GWth during the 1st transient. According to the second transient test, the neutron flux was counted as 1.24×10^{16} n/cm$^2 \cdot$s with FWHM of 136 ms while the maximum power was 5.1 GWth.

E. Transient Test Result Analysis

The transient test results are discussed based on the conversion results in this section. To qualify the accuracy of the measured neutron flux, data from previous research conducted with MPFDs experiments at TREAT in 2017 was used as a reference. The comparison between the converted neutron flux values from the current experiment and the previously reported data allows for a qualitative assessment of the accuracy and reliability of the measurements. The reported neutron flux was 4×10^{11} n/cm$^2 \cdot$ s during the steady-state test with a maximum thermal power of 120 kW [27]. By using the thermal power obtained during the reactor transient tests, which was

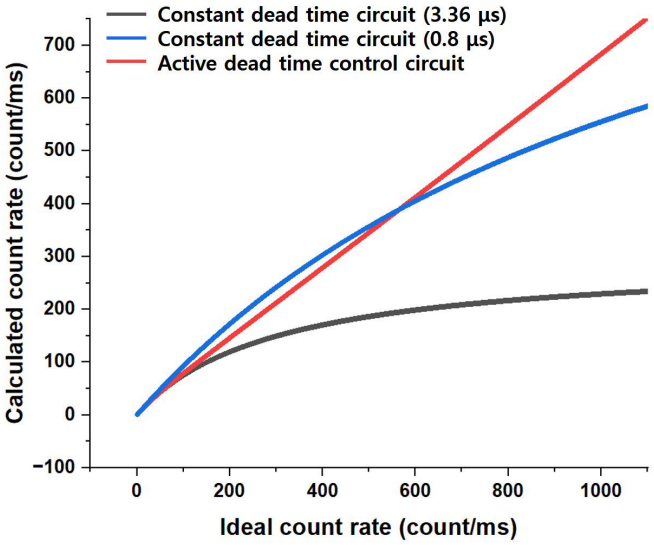

Fig. 13. Comparing the result of calculated count rate. Three cases are analyzed when the dead time is constant at 3.36 and 0.8 μs, and the dead time is actively controlled by the monostable.

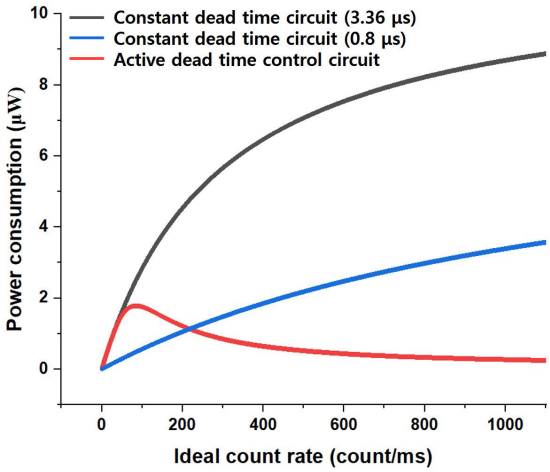

Fig. 14. Comparing results of power consumption. Three cases are analyzed when the dead time is constant at 3.36 and 0.8 μs, and the dead time is actively controlled by the monostable.

2.1 and 5.1 GW, we can convert this neutron flux to be 7.1×10^{15} n/cm$^2 \cdot$s and 1.71×10^{16} n/cm$^2 \cdot$s, respectively. After the conversion process, the error was observed as -1.5% and 38% between the obtained data and the calculated data for comparison at each thermal power, 2.1 and 5.1 GW, respectively. As aforementioned, during the detection process, fission reactions occur, which leads to a reduction in the number of neutron-reactive materials. As a result, the sensitivity of the MPFDs is degraded, which could be a contributing factor to the 38% error observed in the results.

IV. Discussion

A. Comparison of Count Rate

The calculated data for circuits with a constant dead time and ADTC can be calculated using (6) and (14), respectively. The dead time is specified as 3.36 and 0.8 μs, which correspond to the observed maximum and minimum values, respectively, obtained from the monostable circuit during the reactor transient test. Fig. 13 illustrates the calculation results.

The ideal count rate refers to the number of signals generated at the detector within a 1 ms time window. For instance, if the ideal count rate is 650, then the actual count rate would be calculated as 204 (3.36 μs), 427 (0.8 μs) by using (6) in the conventional case. In contrast, ADTC can be calculated as 446 using (14). Consequently, the constant dead time circuit experiences a degradation in the count rate as the number of input signals increases, particularly with increasing dead time. In contrast, the ADTC circuit demonstrates a more linear response to the ideal count rate compared to the constant dead time circuits. Therefore, the proposed preamplifier can compensate for the degradation of the count rate.

B. Power Consumption

In addition to its count rate compensation benefits, the ADTC also offers the advantage of reducing power dissipation. The power consumption during the charge time is proportional to the square of the voltage difference, as described in (3)

$$P = \frac{C}{2}\{V_M - (V_X - V_{\mathrm{DD}})\}^2 = \frac{C}{2}\Delta V^2. \tag{15}$$

Section III-C introduced the conversion method for converting the count data to the neutron flux. In this section, comparisons of count rate and power consumption between the conventional reset circuit and the ADTC circuit are shown. The trigger circuit of the switch for the reset is usually designed using the inverter delay cell array [26]. The delay of the inverter delay cell is calculated as (Y)

$$t_d = \sum_{j=1}^{N} t_{d,j} = 0.69 R_{\mathrm{eq}}(C_{\mathrm{int}} + C_{\mathrm{ext}})N \tag{16}$$

where R_{eq} is an equivalent resistance of the inverter, C_{int} is an internal capacitance, C_{ext} is an external capacitance, and N is the number of inverter stages. To achieve the desired delay, either a large capacitance or a number of inverters is required since the discharge period is determined by the RC time constant. It becomes possible to simplify the modeling process for calculating the count rate and power dissipation, by assuming that the dead time of the monostable circuit remains constant while only the capacitance varies based on the dead time. Therefore, the capacitance is set to 9 and 2.25 pF, corresponding to the dead times of 3.36 and 0.8 μs, respectively. As the remaining charges in the capacitor of the monostable circuit decrease the voltage difference, the power dissipation is also reduced in the high radiation field. Fig. 14 compares the power consumption of the ADTC circuit and constant dead time circuits having 3.36 and 0.8 μs, respectively. Consequently, the ADTC circuit has the lowest power dissipation among the three cases after the ideal count rate of 200.

V. Conclusion

The MPFDs readout system was developed, including the preamplifier with self-reset, the data loggers, and the remote monitoring system. The proposed system can operate in integration and single-event modes. The integration mode

is merged with the conventional current and count modes for radiation detection, where the data logger for integration mode counts the number of saturated outputs of the CSA. On the other hand, the single event mode functions as an analog data logger, capturing and storing data every 1 ms. The monostable circuit is exploited for the self-reset of the preamplifier. The pulsewidth of the monostable output for the self-reset is chosen with sufficient margin to discharge the capacitor stably, regardless of the process variation during fabrication. Thus, the ADTC is introduced to compensate for the longer reset period considered as the dead time of the system. The measured data can be converted from the count rate to the neutron flux using the conversion method. The MPFDs readout system could track the reactor power level as the test result. The conversion results show that the neutron flux is measured as 7.2×10^{15} n/cm^2·s with FWHM of 126 ms and 1.24×10^{16} n/cm$^2 \cdot$s with FWHM of 136 ms at a thermal power of 2.1 and 5.1 GWth, respectively.

REFERENCES

[1] C.-K. Lee, G.-Y. Kwon, and Y.-J. Shin, "Condition assessment of I&C cables in nuclear power plants via stepped-frequency waveform reflectometry," *IEEE Trans. Instrum. Meas.*, vol. 68, no. 1, pp. 215–224, Jan. 2019.

[2] M. Seung, W. Choi, S. Hur, and I. Kwon, "Cold junction compensation technique of thermocouple thermometer using radiation-hardened-by-design voltage reference for harsh radiation environment," *IEEE Trans. Instrum. Meas.*, vol. 71, pp. 1–7, 2022.

[3] M. Alex and M. D. Ghodgaonkar, "Development of an Inconel self powered neutron detector for in-core reactor monitoring," *Nucl. Instrum. Methods Phys. Res. A, Accel. Spectrom. Detect. Assoc. Equip.*, vol. 574, no. 1, pp. 127–132, Apr. 2007.

[4] I. Ramezani and M. B. Ghofrani, "Reconstruction of neutron flux distribution by nodal synthesis method using online in-core neutron detector readings," *Prog. Nucl. Energy*, vol. 131, Jan. 2021, Art. no. 103574.

[5] H. Ding, G. Wu, F. He, J. Tong, and L. Zhang, "Study on the costs and benefits of establishing a unified regulatory guidance for emergency preparedness of small modular reactors in China," *Prog. Nucl. Energy*, vol. 161, Jul. 2023, Art. no. 104722.

[6] D. Shropshire, "Economic viability of small to medium-sized reactors deployed in future European energy markets," *Prog. Nucl. Energy*, vol. 53, no. 4, pp. 299–307, May 2011.

[7] H. Hidayatullah, S. Susyadi, and M. H. Subki, "Design and technology development for small modular reactors—Safety expectations, prospects and impediments of their deployment," *Prog. Nucl. Energy*, vol. 79, pp. 127–135, Mar. 2015.

[8] M. A. Reichenberger et al., "Micro-pocket fission detectors (MPFDs) for in-core neutron detection," *Ann. Nucl. Energy*, vol. 87, pp. 318–323, Jan. 2016.

[9] V. K. Patel, M. A. Reichenberger, J. A. Roberts, T. C. Unruh, and D. S. McGregor, "MCNP6 simulated performance of micro-pocket fission detectors (MPFDs) in the transient REActor test (TREAT) facility," *Ann. Nucl. Energy*, vol. 104, pp. 191–196, Jun. 2017.

[10] M. A. Reichenberger et al., "Fabrication and testing of a 5-node micro-pocket fission detector array for real-time, spatial, iron-wire port neutron-flux monitoring," *Ann. Nucl. Energy*, vol. 110, pp. 995–1001, Dec. 2017.

[11] D. S. McGregor, M. F. Ohmes, R. E. Ortiz, A. S. M. S. Ahmed, and J. K. Shultis, "Micro-pocket fission detectors (MPFD) for in-core neutron flux monitoring," *Nucl. Instrum. Methods Phys. Res. A, Accel. Spectrom. Detect. Assoc. Equip.*, vol. 554, nos. 1–3, pp. 494–499, Dec. 2005.

[12] A. S. M. S. Ahmed, J. K. Shultis, and D. S. McGregor, "Response functions for calculating axial power-density profiles in fuel rods using in-core neutron detectors," *Prog. Nucl. Energy*, vol. 49, no. 5, pp. 385–396, Jul. 2007.

[13] D. M. Nichols et al., "Reactor pulse tracking using micro-pocket fission detectors in research reactors," in *Proc. IEEE Nucl. Sci. Symp. Med. Imag. Conf. (NSS/MIC)*, Oct. 2019, pp. 1–5.

[14] M. A. Reichenberger et al., "Electronic support system enhancements for micro-pocket fission detectors (MPFDs)," in *Proc. IEEE Nucl. Sci. Symp., Med. Imag. Conf. Room-Temperature Semiconductor Detect. Workshop (NSS/MIC/RTSD)*, Oct. 2016, pp. 1–5.

[15] H. Jeon, I. Kwon, and M. Je, "Radiation-hardened sensor interface circuit for monitoring severe accidents in nuclear power plants," *IEEE Trans. Nucl. Sci.*, vol. 67, no. 7, pp. 1738–1745, Jul. 2020.

[16] I. Kwon, T. Kang, B. T. Wells, L. J. D'Aries, and M. D. Hammig, "A high-gain 1.75-GHz dual-inductor transimpedance amplifier with gate noise suppression for fast radiation detection," *IEEE Trans. Circuits Syst. II, Exp. Briefs*, vol. 63, no. 4, pp. 356–360, Apr. 2016.

[17] M. Massarotto, A. Carlosena, and A. J. Lopez-Martin, "Two-stage differential charge and transresistance amplifiers," *IEEE Trans. Instrum. Meas.*, vol. 57, no. 2, pp. 309–320, Feb. 2008.

[18] S. Usman and A. Patil, "Radiation detector deadtime and pile up: A review of the status of science," *Nucl. Eng. Technol.*, vol. 50, no. 7, pp. 1006–1016, Oct. 2018.

[19] M. A. Reichenberger et al., "Fabrication and testing of a 4-node micro-pocket fission detector array for the Kansas State University TRIGA Mk—II research nuclear reactor," *Nucl. Instrum. Methods Phys. Res. A, Accel. Spectrom. Detect. Assoc. Equip.*, vol. 862, pp. 8–17, Aug. 2017.

[20] I. Pázsit, L. Pál, and L. Nagy, "Multiplicity counting from fission chamber signals in the current mode," *Nucl. Instrum. Methods Phys. Res. A, Accel. Spectrom. Detect. Assoc. Equip.*, vol. 839, pp. 92–101, Dec. 2016.

[21] M. Urban and D. Doubravová, "Timepix3: Temperature influence on X-ray measurements in counting mode with Si sensor," *Radiat. Meas.*, vol. 141, Feb. 2021, Art. no. 106535.

[22] I. Kwon, T. Kang, and M. D. Hammig, "Experimental validation of charge-sensitive amplifier configuration that compensates for detector capacitance," *IEEE Trans. Nucl. Sci.*, vol. 63, no. 2, pp. 1202–1208, Apr. 2016.

[23] I. Kwon, T. Kang, B. T. Wells, L. J. D'Aries, and M. D. Hammig, "Compensation of the detector capacitance presented to charge-sensitive preamplifiers using the Miller effect," *Nucl. Instrum. Methods Phys. Res. A, Accel. Spectrom. Detect. Assoc. Equip.*, vol. 784, pp. 220–225, Jun. 2015.

[24] *Nuclear Power Reactor Instrumentation Systems Handbook*, vol. 1, National Technical Information Service (NTIS), Alexandria, VA, USA, 1973.

[25] M. A. Reichenberger, "Micro-pocket fission detectors: Development of advanced, real-time, in-core, neutron-flux sensors," Ph.D. dissertation, Dept. Mech., Nucl. Eng., Kansas State Univ., Manhattan, KS, USA, 2012.

[26] I. Kwon, "Self-reset switching preamplifier for improvement of counting rate," *J. Radiat. Ind.*, vol. 14, no. 1, pp. 9–12, 2020.

[27] W. Fu, "Modeling and simulation of neutron detectors for the transient reactor test facility," Ph.D. dissertation, Dept. Mech., Nucl. Eng., Kansas State Univ., Manhattan, KS, USA, 2019.

Minuk Seung received the B.S. degree in nuclear engineering from Kyunghee University, Yongin, South Korea, in 2019, and the M.S. degree in electrical engineering from Yonsei University, Seoul, South Korea, in 2021, where he is currently pursuing the Ph.D. degree in electrical engineering.

Since 2019, he has been with the Korea Atomic Energy Research Institute (KAERI), Daejeon, South Korea. His research interests include the radiation-hardened analog/mixed-signal design for the radiation detecting system.

Duckhyun Kim received the B.S. degree in electrical engineering from the Korea University of Technology and Education, Cheonan, South Korea, in 2016. He is currently pursuing the M.S. degree in nuclear and quantum engineering with the Korea Advanced Institute of Science and Technology, Daejeon, South Korea.

Since 2016, he has been with the Korea Atomic Energy Research Institute (KAERI), Daejeon. His research interests include integrated circuit design for radiation-hardened design of digital to analog converters and radiation detecting systems.

Dongseong Shin received the B.S. degree from Hanbat National University, Daejeon, South Korea, in 2016.

From 2017, he joined the Korea Atomic Energy Research Institute (KAERI), Daejeon. His research interests include the software design for nuclear I and C and wireless systems.

Troy C. Unruh received the B.S. degree in mechanical and nuclear engineering and the M.S. degree in nuclear engineering from Kansas State University, Manhattan, KS, USA, in 2004 and 2009, respectively.

He is the Manager with the Department of Measurement Science, Idaho National Laboratory and the technical point of contact for the area of sensors for advanced reactors in the advanced sensor and instrumentation program, which is an element of the Department of Energy Nuclear Energy Enabling Technology portfolio. He has more than 15 years' experience with reactor operations, reactor experiments, and the development and testing of sensors for nuclear reactors. His research interests include the development of in-core instrumentation technology, specializing in fabrication, testing, and analysis of prototypic sensor and instrumentation of use in irradiation tests of fuels and materials and in the demonstration of advanced reactor concepts.

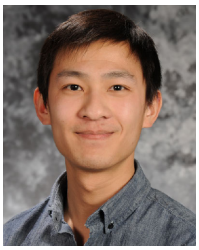

Kevin Tsai received the B.S. degree in physics and mathematics, and the M.S. degree in nuclear science and engineering from Idaho State University, Pocatello, ID, USA, in 2014 and 2018, respectively.

In 2018, he joined as a Nuclear Instrumentation Engineer with the Measurement Sciences Department, Idaho National Laboratory, Idaho Falls, ID, USA. He currently leads the development and deployment of in-pile neutron flux sensors with a specific focus on the self-powered neutron detectors under the DOE nuclear energy enabling technology advanced sensors and instrumentation program. He has been serving as the Program's Technical Lead for conducting in-pile sensor testing at the transient reactor test (TREAT) facility and has extensive hands-on experience deploying sensors in TREAT, since April 2018.

Woo-Young Choi (Member, IEEE) received the B.S., M.S., and Ph.D. degrees in electrical engineering and computer science from the Massachusetts Institute of Technology, Cambridge, MA, USA, in 1986, 1988, and 1994, respectively.

From 1994 to 1995, he was a Post-Doctoral Research Fellow with NTT Opto-Electronics Laboratories, Chiyoda, Japan. In 1995, he joined the Department of Electrical and Electronic Engineering, Yonsei University, Seoul, South Korea, where he is currently a Professor. His research interests include high-speed circuits and systems that include high-speed electronic circuits, optoelectronics, and optical interconnects.

Inyong Kwon (Member, IEEE) received the B.S. degree in electrical engineering from Yonsei University, Seoul, South Korea, in 2010, and the M.S. and Ph.D. degrees in electrical engineering and computer science from the University of Michigan, Ann Arbor, MI, USA, in 2012 and 2015, respectively.

He is an Assistant Professor of radiological science with Yonsei University and the Director with the Integrated Circuit for Radiation Laboratory (ICR), Wonju, South Korea. He has held Research Staff positions at the Stanford University, Stanford, CA, USA, and the Korea Atomic Energy Research Institute (KAERI), Daejeon, South Korea, and a Professorships at the University of Science and Technology (UST), Daejeon. His research interests include integrated circuit design for radiation sensing and hardening that can be used in extreme and specific environments such as nuclear power plants, space, and advanced medical instruments.